Available online at www.sciencedirect.com

ScienceDirect

Energy Procedia 69 (2015) 388 – 397

Energy Procedia

International Conference on Concentrating Solar Power and Chemical Energy Systems
SolarPACES 2014

Preliminary design and performance analysis of a multi-megawatt scale dense particle suspension receiver

A. Gallo[a], J. Spelling[a,*], M. Romero[a], J. González-Aguilar[a]

[a] *High Temperature Processes Unit, IMDEA Energy Institute, 28935 Móstoles, Spain*

Abstract

A novel receiver concept is presented, based on the use of a dense particle suspension as the heat transfer medium; this medium allows receiver operation at high temperatures (above 650°C), resulting in significant gains in power plant efficiency. A 10 MW_{th} receiver has been designed based on the scale-up of a 150 kW_{th} prototype currently undergoing testing. The predicted thermal efficiency is 81.3%, well above the design target of 70%. Material temperatures within the absorber tubes were maintained below 850°C throughout the receiver, below the limits of high temperature steels.

Peer review by the scientific conference committee of SolarPACES 2014 under responsibility of PSE AG

Keywords: dense particle suspension; high temperature; solid particle receiver; high efficiency solar power

1. Introduction

Contemporary concentrating solar power (CSP) plants are still largely based on parabolic trough technology, developed nearly 30 years ago, and only limited progress has been made on driving down costs. These parabolic trough power plants employ Rankine-cycle power blocks with low temperature (< 400ºC) steam turbines which operate with relatively low efficiencies (~35% when dry-cooled [1]). Reaching higher temperatures is seen as key to future cost reductions, as higher temperatures lead to both higher power conversion efficiencies and increased storage densities, directly reducing the total cost of the solar collector field and the specific cost of the storage units.

* Corresponding author. Tel.: +34-91-737-1150; fax: +34-91-737-1140.
E-mail address: james.spelling@imdea.org

Peer review by the scientific conference committee of SolarPACES 2014 under responsibility of PSE AG
doi:10.1016/j.egypro.2015.03.045

In recent years, two competing technologies have emerged to achieve higher temperatures, namely molten-salt and direct steam generation towers [2], which have cycle efficiencies in region of 40%, leading to reduced costs. Despite this, both technologies have their associated drawbacks. Molten-salt systems are limited to operating temperatures below 550°C by the thermal stability of the salt itself, preventing the use of even more efficient, higher temperature power conversion cycles. Molten-salt systems also suffer from freezing problems if the salt temperature drops too low, resulting in a high parasitic power consumption for heat-tracing. Direct steam systems are not limited in the temperatures they can achieve, as no intermediary heat transfer fluid is used. However, they typically operate with steam temperatures in the region of 565°C and no cost-effective large-scale storage system has been developed for live steam. Use of this technology therefore negates the key advantages of solar thermal power: the ability to store energy [2]. As such, if the true potential of CSP technology is to be unlocked, new heat transfer media (HTM) are needed that can both reach higher temperatures and easily be stored. This paper addresses the design of a multi-megawatt scale receiver using one such HTM: the dense gas-particle suspension.

Nomenclature

c	Specific heat	[J/kgK]
d_p	Particle diameter	[m]
E	Electrical power	[W]
f_p	Particle packing factor	[-]
G	Mass flux	[kg/m^{2}s]
M	Mass flow rate	[kg/s]
P	Pressure	[Pa]
Q	Thermal power	[W]
T	Temperature	[K]
u	Flow speed	[m/s]
α	Heat transfer coefficient	[W/m^{2}K]
ε	Emissivity	[-]
η	Component efficiency	[-]
λ	Thermal conductivity	[W/mK]
μ	Viscosity	[Pa·s]
ρ	Density	[kg/m^3]
φ_p	Particle volume fraction	[-]

2. Novel heat transfer media for solar thermal power plants

A wide range of alternative high-temperature HTM have been studied for use in CSP plants, including gases, improved molten salts and solid particles [3], as shown in Table 1. In principle, the simplest solution would appear to be to develop new molten salt materials that are capable of resisting higher temperatures; in this way existing receiver technology could be used, reducing the required investment. However, in order to overcome the temperature limitations imposed by the nitrate salts currently used in CSP plants [4] it is necessary to switch to carbonate or chloride salts, which suffer from corrosion issues at high temperatures [5], significantly increasing maintenance costs. The use of inert gases (e.g. air, helium, etc.) as the HTM is an alternative, eliminating the thermal decomposition and corrosion problems. However, gases suffer from poor heat transfer properties which poses challenges for receiver design, while their low densities complicate the integration of energy storage.

The use of solid particles as the HTM is another option, capable of reaching temperatures of 1000°C when ceramic particles are used [6]. Solid particle HTM are also ideally suited for storage applications, which can be easily implemented through simple bulk storage of hot particles. The solid particles are typically directly irradiated by the concentrated sunlight, allowing for very high heat fluxes as there is no interposing material to limit heat transfer. However, this approach leads to high heat losses (thermal efficiencies < 50% under real conditions [7]) and significant difficulties in controlling the flow of loose particles within the receiver.

Table 1: Comparison of high temperature solar heat transfer media [3].

Medium	Temperatures	Advantages	Disadvantages
Molten Salts	> 600°C	Good heat transfer Proven concept Easy to store	Salt freezing Corrosion
Gases	> 800°C	High temperatures Easy fluid handling	Poor heat transfer Low heat fluxes Difficult to store
Solid Particles	> 800°C	Very high temperatures Very high heat fluxes Easy to store	High heat losses Difficult fluid handling

The dense particle suspension (DPS) is an alternative to the classical solid particle HTM studied previously, combining the good heat transfer properties of liquids and the ease of handling of gases with the high temperature properties of solid particles. The DPS consists of very small (μm-scale) particles which can be fluidized at low gas speeds (group A of Geldart's classification [8]); these fluidized particles can then be easily transported in a similar manner to a gas. The fraction of particles within the fluidized suspension is high (up to around 40% by volume [9]), resulting in a HTM with a high apparent density (above 1000 kg/m^3 [9]), similar to that of a liquid, and a significant improvement in heat transfer compared to the entraining gas alone (with heat transfer coefficients in the range of 500 to 750 W/m^{2}K [10]).

If ceramic particles are considered, particle suspensions can be used at extremely high temperatures (up to 1000°C [6]), limited only by the material of the absorber tubes. Furthermore, ceramic particles are chemically inert and present no risk of explosion. As the particles are solid, they cannot freeze, removing the lower temperature limit associated with molten salts and eliminating problems with heat tracing. This results in a large temperature range being available for DPS systems, which increases the storage density, reducing costs and simplifying storage tank design. However, the design of heat exchangers to recover heat from the stored particles remains a challenge.

3. Characteristics of the dense particle suspension

The DPS is entrained by a gas flow (which in this case is simply air) which maintains the particle flow in a fluidized state: the upwards flow of the gas acts to overcome the effects of gravity on the solid particles through drag forces. As such, the upward velocity of the particles u_p is always less than the velocity of the gas u_g, as a certain slip velocity u_{slip} is required in order to generate the necessary drag force; as shown schematically in Fig. 1. According to experiments performed by CNRS [10], the slip velocity between the gas and particles is more-or-less equal to the minimum fluidization velocity u_{mf} regardless of the flow conditions. The velocity of the particles within the DPS can therefore be calculated as $u_p = u_g - u_{mf}$.

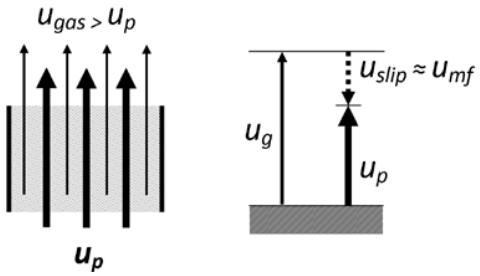

Fig. 1. Gas and particle velocities in the dense particle suspension.

3.1. Thermophysical properties of the dense particle suspension

In order to model the absorption and transfer of heat by the DPS, it is necessary to determine the bulk properties of this novel HTM, which are chiefly dependent on the volume fraction of particles in the suspension: φ_p. Given the large difference in density between the particles and the gas (a factor of around 5000 for air at 500°C and

atmospheric pressure), the overall density ρ_{DPS} of the suspension depends strongly on the concentration of particles, and can be determined using Equation (1) as a function of the densities of the particles ρ_p and the gas ρ_g. The addition of solid particles to the gas flow greatly increases the apparent density of the HTM, allowing a large mass flow to be transported at low flow speeds.

$$\rho_{DPS} = \varphi_p \rho_p + (1-\varphi_p)\rho_g \tag{1}$$

The mass flux G_{DPS} of the suspension (mass flow per unit area) cannot be calculated directly from its density, due to the difference in flow speed of the two media and Equation (2) must be used instead. Due to the high density of the solid particles, and the low difference in speed between the two media (u_{mf} = 5.5 mm/s for 63.9 μm particles) the overall mass flux is strongly determined by the fraction of particles.

$$G_{DPS} = \varphi_p \rho_p (u_g - u_{mf}) + (1-\varphi_p)\rho_g u_g \tag{2}$$

The specific heat capacity of the suspension $c_{p,DPS}$ can be calculated using Equation (3) as a function of the heat capacity of the particles $c_{p,p}$ and the gas $c_{p,g}$. The difference in heat capacities between the particles and the gas is not as significant as the difference in densities (only a factor of 1.05 at 500°C); as such it is the density increase that is responsible for the improved heat transport properties of the suspension.

$$c_{p,DPS} = \frac{\varphi_p \rho_p c_{p,p} + (1-\varphi_p)\rho_g c_{p,g}}{\varphi_p \rho_p + (1-\varphi_p)\rho_g} \tag{3}$$

The effective thermal conductivity of the suspension λ_{DPS} can be estimated using the Maxwell model [11], given in Equation (4) as a function of the conductivity of the particles λ_p and the gas λ_g. The difference in thermal conductivity between the two media is again very significant (a factor of around 2000 at 500°C), however, as the two conductivities operate largely in series, the increase in thermal conductivity for the suspension is relatively modest (a factor of only 2.3 for a suspension consisting of 35 % particles).

$$\frac{\lambda_{DPS}}{\lambda_g} = 1 + \frac{3 \cdot \varphi_p (f_\lambda - 1)}{1 + f_\lambda - \varphi_p (f_\lambda - 1)} \quad \text{where} \quad f_\lambda = \frac{\lambda_p}{\lambda_g} \tag{4}$$

The apparent viscosity of the suspension μ_{DPS} can be calculated using the model of Brouwers [12], given in Equation (5) as a function of the gas viscosity μ_g and the packing density factor f_ρ, which takes a value of 0.64 for randomly packed uniform spheres. The apparent viscosity of the suspension increases exponentially with the volume fraction of particles (giving a factor of 5 for a suspension consisting of 35 % particles); however, due to the slow flow speed of the suspension, friction losses in the system remain low.

$$\frac{\mu_{DPS}}{\mu_g} = \left(f_\rho \cdot \frac{1-\varphi_p}{f_\rho - \varphi_p} \right)^{\frac{2.5 f_\rho}{1-f_\rho}} \tag{5}$$

3.2. Heat transfer in the dense particle suspension

The addition of particles to the fluidization medium results in a significant improvement in heat transfer properties when compared to the gas alone. A key parameter for the analysis of heat transfer in fluidized systems is the Archimedes number Ar, a dimensionless number which can be calculated using Equation (6) as a function of the particle size d_p, the viscosity of the entraining gas μ_g and the gas and particle densities, ρ_p and ρ_g respectively.

$$\mathrm{Ar} = \frac{g\rho_g d_p^3}{\mu_g^2}\left(\rho_p - \rho_g\right) \tag{6}$$

A number of different correlations exist to calculate the maximum convective heat transfer coefficient α_{max} between the DPS and the walls of the enclosing tubes [13]. Three of the most common correlations have been selected for use in the design of the particle suspension receiver and are given in Equations (7), (8) and (9), where the Nusselt number is defined as $\mathrm{Nu} = \alpha \cdot d_p/\lambda_g$ and the Prandtl number as $\mathrm{Pr} = c_{p,\mathrm{DPS}} \cdot \mu_{\mathrm{DPS}}/\lambda_{\mathrm{DPS}}$.

$$\mathrm{Nu}_{\mathrm{Khan}}^{max} = 0.157 \cdot \mathrm{Ar}^{0.475} \tag{7}$$

$$\mathrm{Nu}_{\mathrm{Zabrodsky}}^{max} = 35.8 \cdot \frac{\rho_p^{0.2} \cdot d_p^{0.64}}{\lambda_g^{0.4}} \tag{8}$$

$$\mathrm{Nu}_{\mathrm{Baskakov}}^{max} = 0.72 \cdot \mathrm{Ar}^{0.2}\,\mathrm{Pr}^{0.33} \tag{9}$$

None of these correlations take into account radiation heat transfer between tube walls and the particles, which can be a significant contribution at high temperatures [14]. The radiation heat transfer coefficient can be calculated using Equation (10), as a function of the emissivity of the particles and the tube walls, ε_p and ε_t respectively, and the mean temperature of the absorber and suspension T_{mean}. The overall heat transfer coefficient α within the absorber can then be calculated for the two cases above using Equation (11), where the mean convective heat transfer coefficient is assumed to be equal to 70% of the maximum value, based on the recommendations of Khan [13].

$$\alpha_{rad} = 7.3 \cdot \varepsilon_p \varepsilon_t \sigma T_{mean}^3 \tag{10}$$

$$\alpha = 0.7 \cdot \alpha_{max} + \alpha_{rad} \tag{11}$$

In addition to the analytical correlations presented above, heat transfer experiments have been performed on the DPS by CNRS [10] as part of the Concentrated Solar Power in Particles (CSP2) project [15], allowing heat transfer to be correlated with the mass flux of the DPS. Taking into consideration the four different heat transfer approaches presented, a representative mean value α_{DPS} needs to be obtained. A geometric mean value is used, which gives additional weight to the lowest value and results in a conservative approximation of the heat transfer coefficient.

4. Receiver specifications

The DPS solar receiver concept considered in the CSP2 project [15] is shown in Fig. 2. Cold particles are taken from a storage hopper and conveyed to an air-driven fluidized bed. The fluidized particles pass up through the absorber tubes onto which the concentrated solar flux is focused, heating the particles to the desired temperature. Upward flow of the particles has been selected as it increases controllability of the system, and allows the residence time of the particles within the receiver to be easily modified to achieve the desired outlet temperature. A 100 $\mathrm{kW_{th}}$ prototype receiver based on this concept is currently being tested at the PROMES facility in Odeillo [10].

This paper presents the scale-up of the DPS receiver concept to 10 $\mathrm{MW_{th}}$, in order to examine the characteristics of a receiver that is suitable for utility-scale applications. Before this process begins, it is necessary to fix certain key parameters for the scale-up design, which are shown in Table 2 along with the most important limits associated with the system. A cavity geometry has been selected for the receiver with an opening angle of 135°, within which the particles are heated from 150 to 650°C. The CSP2 project has set a target efficiency of 70% for the DPS receiver. In the current project, silicon carbide particles are considered [16], with the characteristics shown in Table 3.

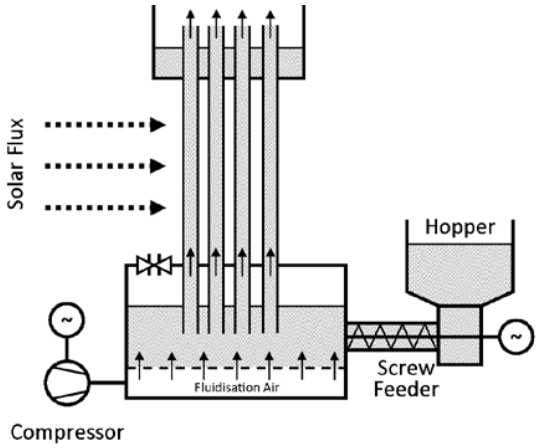

Fig. 2. Schematic illustration of the dense particle receiver.

Table 2. Receiver design parameters.

	Design Parameters	Value	Limit	
φ_p	Particle Volume Fraction at Inlet	35	*< 63*	[%]
u_g	Gas Flow Velocity at Inlet	40	*< 200*	[mm/s]
d_i	Absorber Tube Inner Diameter	64	*< 100*	[mm]
t_t	Tube Wall Thickness	4	-	[mm]
λ_t	Tube Conductivity (at 500°C)	21.5	-	[W/mK]
α_t	Tube Absorptivity (at 500°C)	0.90	-	[-]
ε_t	Tube Emissivity (at 500°C)	0.85	-	[-]

Table 3. Particle characteristics.

	Particle Characteristics	Value	
d_p	Sauter Mean Diameter	63.9	[µm]
ρ_p	Density	3210	[kg/m^3]
u_{mf}	Minimum Fluidization Velocity	5.5	[mm/s]
$c_{p,p}$	Specific Heat Capacity (at 500°C)	1150	[J/kgK]
λ_p	Thermal Conductivity (at 500°C)	109	[W/mK]

5. Receiver design procedure

Having established the receiver specifications and the physical properties of the DPS, a global heat transfer analysis of the absorber tubes can now be performed in order to determine the geometry of the receiver.

5.1. Mass flow calculation

Assuming that the entraining air used to fluidize the particles is simply vented after passage through the receiver, the net *useful* thermal power absorbed is the energy increase of the particles alone. The mass flow of particles M_p through the receiver required to absorb a given thermal power Q_{use} can be calculated using Equation (12), where $T_{p,in}$ and $T_{p,out}$ are the inlet and output temperatures of the particles, respectively.

$$\dot{M}_p = \frac{\dot{Q}_{use}}{c_{p,p}\left(T_p^{out} - T_p^{in}\right)} \tag{12}$$

In order to drive the flow of particles through the receiver, a certain mass flow of gas M_g is also required, which can be calculated using Equation (13) based on the characteristics of the gas and the DPS flow. The gas flow, whilst absorbing heat during passage through the receiver, does not have its energy harnessed by the CSP plant, and will therefore constitute an additional source of thermal losses.

$$\dot{M}_g = \frac{\left(1-\varphi_p\right)\rho_g u_g}{\varphi_p \rho_p \left(u_g - u_{mf}\right)} \cdot \dot{M}_p \tag{13}$$

5.2. Parasitic power consumption

In order to drive the DPS through the receiver, a certain pressure must be maintained in the fluidization chamber at the base of the receiver (see Fig. 2). The required pressure P_{base} at the inlet of the receiver must be sufficient to overcome the combination of the hydrostatic pressure of the DPS column and the friction losses within the tubes; this can be calculated using Equation (14), where P_a is the atmospheric pressure. Due to the high density of the DPS and the very low flow speeds, hydrostatic effects are strongly dominant.

$$P_{base} = P_a + g\rho_{\mathrm{DPS}} h_t + 0.184 \cdot \left(\frac{G_{\mathrm{DPS}} d_i}{\mu_{\mathrm{DPS}}}\right)^{-0.2} \frac{h_t}{d_i} \cdot \frac{G_{\mathrm{DPS}}^2}{2\rho_{\mathrm{DPS}}} \tag{14}$$

The power consumption E_{comp} of the compressor used to drive the fluidizing air flow can be calculated using Equation (15), as a function of the ambient temperature T_a, as well as the polytropic and mechanical efficiencies of the compressor unit, η_p and η_{mec} respectively. The power consumption E_{screw} of the screw feeder that delivers particles to the fluidization chamber can be calculated using Equation (16). Additional power will also be needed to lift the particles against gravity to the top of the tower.

$$\dot{E}_{comp} = \frac{\dot{M}_g c_{p,g} T_a}{\eta_{mec}} \left(\left(\frac{P_{base}}{P_a} \right)^{\frac{r_g}{\eta_p c_{p,g}}} - 1 \right) \tag{15}$$

$$\dot{E}_{screw} = \frac{\dot{M}_p \left(P_{base} - P_a\right)}{\eta_{mec} f_\rho \rho_p} \tag{16}$$

5.3. Global heat transfer in the absorber tubes

Due to the fact that the incident solar radiation will only impact the absorber tubes on one side, the temperature distribution in the metal will not be uniform. A hotter zone will form on the side absorbing the radiation and heat will conduct away from this zone around the circumference of the tubes, exchanging heat with the fluid at a lower temperature. As such, the rate of heat transfer is reduced compared to the case where the whole tube is at the same peak surface temperature.

Using the analogy presented in Fig. 3, the lateral conductive zones can be modelled as heat transfer fins, effectively increasing the heat transfer rate from the frontal active zone. Using the principal of heat transfer symmetry [17], it can be deduced that no heat will be transferred circumferentially at the back of the tube. The two

lateral sides of the tubes can therefore be considered as two separate fins with adiabatic tips, and the overall heat transfer rate U from the tube to the particle suspension can be calculated using Equation (17), where f_{act} is the active frontal fraction of the tube, λ_t the thermal conductivity of the tube, d_i the internal tube diameter, t_t the thickness of the tube walls and α_{DPS} the bulk heat transfer coefficient of the DPS flow.

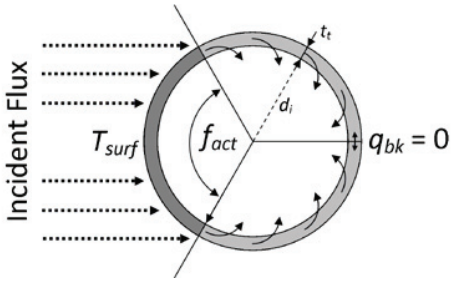

Fig. 3. Circumferential heat transfer zones within the absorber tubes.

$$U = f_{act} \cdot \alpha_{DPS} + 2 \cdot \frac{\sqrt{\alpha_{DPS} \lambda_t t_t}}{\pi d_i} \tanh\left(\pi \left(d_i + \frac{t_t}{2} \right) \left(\frac{1 - f_{act}}{2} \right) \sqrt{\frac{\alpha_{DPS}}{\lambda_t t_t}} \right) \quad (17)$$

5.4. Radiative flux on the absorber surface

In order to be able to design the DPS receiver, it is necessary to know the flux distribution on the absorber surface. This flux distribution depends upon the layout of the heliostat field as well as on the geometry of the absorber itself. The heliostat field for the 10 MW_{th} receiver has been designed using WINDELSOL [18], and is shown in Fig. 4. A total of 1063 heliostats are required, each with an individual surface area of 20 m^2, and the central tower measures 65 m in height; the nominal efficiency of the heliostat field is 78.0%. The nominal flux profile on the absorber is shown in Fig. 5. As the geometry of the receiver is needed in order to determine the flux profile, which in turn is needed to design the receiver, an iterative approach has been used. A first receiver design is elaborated assuming a uniform flux distribution, the geometry of this receiver is then sent to WINDELSOL in order to obtain the flux distribution at the absorber; a new receiver design is then generated, and the process continues until a converged design is reached.

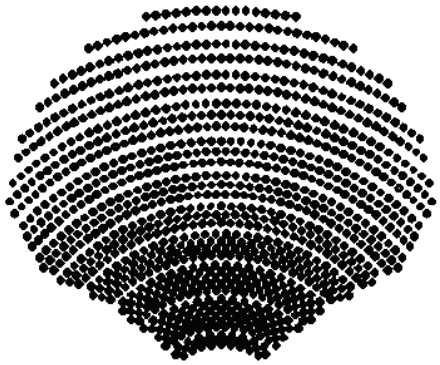

Fig. 4. Heliostat field layout.

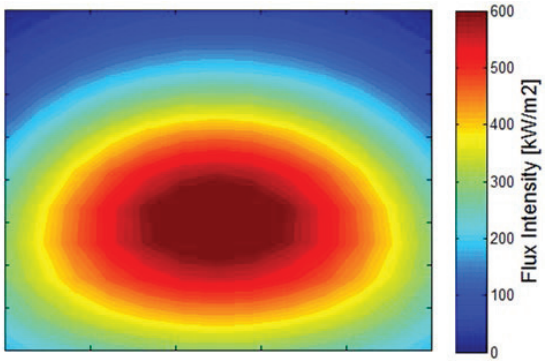

Fig. 5. Flux profile on absorber surface.

6. Receiver design results

The final geometry of the 10 MW_{th} receiver can now be established and is shown in Fig. 6. Consisting of an array of 150 absorber tubes, each with a height of 4.6 m and coated with Pyromark Series 2500 high-temperature paint

[19], the cavity has an aperture area of 39.0 m^2. In total, 67.3 t/hr of particles flow through the receiver, carried by 29.5 kg/hr of air, a mass ratio of 2281:1. The aspect ratio of the receiver is in the region of 1.85:1, resulting in a relatively stretched design. The surface temperature of the absorber at nominal load is shown in Fig. 7. The peak surface temperature is 837°C, which is below the limit of high temperature steels [20]; as the DPS is fluidized using ambient air, pressure loading on the tubes will be negligible.

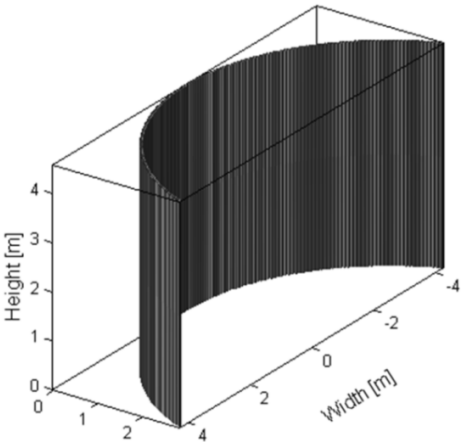

Fig. 6. Cavity geometry.

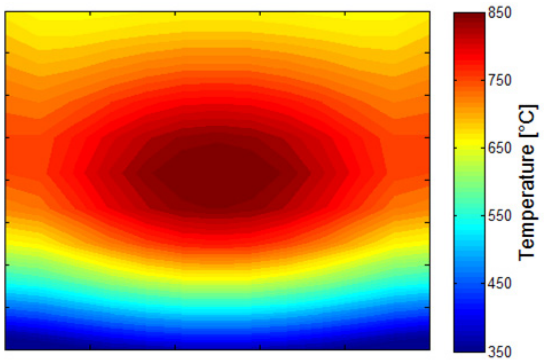

Fig. 7. Absorber surface temperature.

As shown in Table 4, heat losses from the receiver are dominated by radiation and convection losses, resulting in a design-point efficiency of 81.3%, well above the 70% target. Heat losses from venting of the entraining air are almost negligible, at 0.04% of the total input power; as such, venting of the air from the receiver does not penalize performance, as long as effective measures are taken to separate the particles from the flow. Parasitic consumption for the 10 MW_{th} receiver amounts to a total of 19.7 kW_e, of which 18.9 kW_e are for particle transport; the air compressor consumption is only 0.8 kW_e.

Table 4. Receiver thermal performance.

	Design Parameters	Value		Relative	
Q_{field}	Total Input Power from Field	12297	[kW]	100.0	[%]
Q_{rad}	Radiation Losses	1239	[kW]	10.1	[%]
Q_{conv}	Convection Losses	746	[kW]	6.1	[%]
Q_{refl}	Reflection Losses	307	[kW]	2.5	[%]
Q_{vent}	Air Venting Heat Losses	5	[kW]	< 0.1	[%]
Q_{use}	Total Useful Heat	10000	[kW]	81.3	[%]

7. Conclusions

A thermal model of a novel solid particle receiver has been developed and used for the preliminary design of a 10 MW_{th} cavity receiver. The model predicts good performance for the design, with a thermal efficiency in excess of 80% and peak surface temperatures below the material limits. Heliostat field design has been performed using the WINDELSOL tool and coupled with the design process, in order to allow realistic flux distributions to be used when designing the receiver. Results from the thermal analysis of this novel design can now be integrated into system studies in order to determine the performance of the complete CSP plant.

However, while the design of the 10 MW_{th} particle receiver is promising, it represents only a first step in the scale-up process. An output of 10 MW_{th} will result in a net power plant output in the region of 2 to 3 MW_e, which is far below typical CSP plants sizes, which are currently between 50 and 100 MW_e. The key challenge for continued

scale-up is that the speed of the gas within the tubes is constrained by the need to maintain correct fluidization conditions, which limits the achievable mass flux. A limit of 40 kg/m^{2}s was considered in this work, however it is hoped that future results will validate the use of higher fluxes; values up to 700 kg/m^{2}s are theoretically achievable.

With the current mass flux limit, the receiver design becomes increasingly stretched as the power output increases, posing challenges for heliostat aiming. Alternative designs may be required at larger powers, such as multi-unit receivers, mounted in parallel on the central tower. The economies of scale obtained from building larger power plants should help to offset the added cost of these more complex designs. Further scale-up and optimization of the receiver design will be pursued as additional results become available from the CSP2 project.

Acknowledgements

This work has been co-funded by the European Commission as part of the Concentrated Solar Power in Particles project (CSP2, FP7 project number: 282932), the support of which is gratefully acknowledged. Additional thanks are given to our partners in the CSP2 project for their valuable feedback and advice on this work.

References

[1] A. Fernández-García, E. Zarza, L. Valenzuela et al., *Parabolic-Trough Solar Collectors and their Applications*, Renewable and Sustainable Energy Reviews, Volume 14/7 (2010), pp. 1695 – 721

[2] M. Romero, J. González-Aguilar, *Solar Thermal CSP Technology*, WIREs Energy and Environment, Volume 3 (2014), pp. 42 – 59

[3] C. Ho, B. Iverson, *Review of High-Temperature Central Receiver Designs for Concentrating Solar Power*, Renewable and Sustainable Energy Reviews, Volume 29 (2014), pp. 835–46

[4] E. Freeman, *The Kinetics of the Thermal Decomposition of Sodium Nitrate and of the Reaction between Sodium Nitrate and Oxygen*, Journal of Physical Chemistry, Volume 60 (1956), pp. 1487–93

[5] A. Kruizenga, 2012, *Corrosion Mechanisms in Chloride and Carbonate Salts*, Sandia National Laboratories (SAND2012-7594)

[6] P. Falcone, J. Noring, J. Hruby, 1985, *Assessment of a Solid Particle receiver for a High Temperature Solar Central Receiver System*, SANDIA National Laboratories (SAND85-8208)

[7] P. Siegel, C. No, S. Khalsa et al., *Development and Evaluation of a Prototype Solid Particle Solar Receiver: On-Sun Testing and Model Validation*, Transactions of the ASME, Journal of Solar Energy Engineering, Volume 132 (2010)

[8] D. Geldart, 1973, *Types of Gas Fluidization*, Power Technology, Volume 7, pp. 285 – 92

[9] G. Flamant, D. Gauthier, H. Benoit et al., *A New Heat Transfer Fluid for Concentrating Solar Systems: Particle Flow in Tubes*, International SolarPACES Conference, Energy Procedia, Volume 49 (2014), pp. 617 – 26

[10] G. Flamant, D. Gauthier, H. Benoit et al., *Dense Suspension of Solid Particles as a New Heat Transfer Fluid for Concentrated Solar Thermal Plants: On-Sun Proof of Concept*, Chemical Engineering Science, Volume 102 (2013), pp. 567–76

[11] A. Cherkasova, 2009, *Thermal Conductivity Enhancement in Micro- and Nano-Particle Suspensions*, PhD Thesis, State University of New Jersey, New Brunswick

[12] H. Brouwers, *Viscosity of a Concentrated Suspension of Rigid Monosized Particles*, Physical Review E, Volume 81 (2010)

[13] O. Molerus, K. Wirth, 1997, *Heat Transfer in Fluidized Beds*, Particle Technology Series, Springer

[14] A. Baskakov, O. Panov, *Comparison of Maximum Coefficients of Heat Transfer to a Surface Submerged in a Fluidized Bed with an Estimate Obtained from an Empirical Formula*, Journal of Engineering Physics, Volume 45 (1983), pp. 1357 – 62

[15] Concentrated Solar Power in Particles: http://www.csp2-project.eu/

[16] S. Touloukian (editor), 1967, *Thermophysical Properties of High Temperature Solid Materials*, Volume 5, Part 1, pp. 123-129, MacMillan Co., New York

[17] F. Incropera, D. De Witt, T. Bergman et al., 2007, *Fundamentals of Heat and Mass Transfer*, Sixth Edition, John Wiley & Sons, New York

[18] AICIA-CIEMAT-SOLUCAR, 2002, *WINDELSOL 1.0 Users Guide*

[19] C. Ho, J. Pacheco, 2014, *A Levelized Cost of Coating Metric for Evaluation of Solar Selective Absorber Materials*, Proceedings of the International SolarPACES Conference, Sept. 16 – 20, Beijing

[20] British Stainless Steel Association, *Maximum Service Temperatures in Air for Stainless Steels*, retrieved from http://www.bssa.org.uk (accessed 5th June 2014)